ROYAL SOCIETY
OF CHEMISTRY

PAPER

Check for updates

Hydrogen production from CO_2 reforming of methane using zirconia supported nickel catalyst†

Abdulrahman N. Kurdi, Ahmed A. Ibrahim,* Ahmed S. Al-Fatesh, [ID] *
Abdullah A. Alquraini, Ahmed E. Abasaeed and Anis H. Fakeeha

The use of hydrogen as an alternative fuel is an attractive and promising technology as it contributes to the reduction of environmentally harmful gases. Finding environmentally friendly cheap active metal-based catalysts for H_2 rich syngas *via* dry reforming of methane (DRM) for industrial applications has posed a challenge. In this paper, H_2 production *via* CO_2 reforming of methane was investigated over $5Ni/ZrO_2$ catalysts. The catalytic performance of all prepared catalysts was evaluated in a microtubular fixed bed reactor under similar reaction conditions (*i.e.*, activation temperature at 700 °C, feed flow rate of 70 ml min^{-1}, reaction temperature 700 °C for 440 min reaction time) of CO_2 reforming of methane. Different characterization techniques such as; BET, CO_2-TPD, TGA, XRPD, Raman, and TEM, were used. The study of the textural properties of catalysts established that the BET of pristine catalyst (5NiZr) was enhanced by the addition of modifiers and promoters. A bimodal TPR distribution in the reduction temperature range of 250−550 °C was recorded. In the CO_2-TPD analysis, the strength of basicity came in this order: 5Ni15YZr > 5Ni10YZr > 5Ni5YZr > 5NiZr > 5Ni20YZr. The investigation of catalyst modifiers (MgO and Y_2O_3) resulted in the Y_2O_3 modifier improving the activity and catalytic performance better than MgO, which generated a hydrogen yield of 22%. 15% Y_2O_3 modifier loading gave the highest H_2 yield 53% in the phase of different loadings of yttria. The study of the influence of promoters (Cs, Ga, and Sr) revealed that the catalytic performance of 5Ni15YZr catalysts promoted with Sr towards the H_2 yield enhanced the activity to 62%. The promoted catalysts displayed lower carbon deposition compared to the unpromoted catalyst, which provided 25.6 wt% weight loss.

1. Introduction

Almost 85% of the total world's energy is coming from fossil fuels. Yet the global demand for energy, obtained from coal and fossil oils, is growing and this has a negative influence on the environment causing global warming, acid rain, greenhouse gas (GHG) emissions, climate change, and ozone holes.[1,2] According to the agreement of the Kyoto Protocol, and the Paris Agreement on climate change, the major greenhouse gases are nitrogen oxides, carbon dioxide, methane, hydro-fluorocarbon, per-fluorocarbon, and sulfur hexafluoride.[3,4] More attention needs to be paid to CO_2 and CH_4 because they are chiefly responsible for global warming. Increasing the worldwide consumption of electricity needs the development of exact intelligent methods and algorithms for its projection. Among the techniques is the genetic algorithm which optimizes and uses stochastic search.[5] G. Aydin *et al.*,

modeled the coal consumption and its future demand in turkey using trend analysis.[6] In another work, the investigators elaborated on the major sources of methane emissions in energy production and its mitigation options from the energy sector.[7] In the light of all obstacles that emerged from using fossil fuels, hydrogen, as a transportation fuel and a chemical for industry,[8] has drawn immense attention due to its high specific energy density.[9] Hydrogen is an environmentally friendly fuel, which can be used for powering engines, producing electricity, and for other numerous industrial applications.[10] There are many sources for producing hydrogen mostly sustainable ones like biomass, water, coal, oil, and natural gas with different processes of production.[11] The conversion of methane or different hydrocarbons to hydrogen-rich syngas (admixture of carbon monoxide and hydrogen) is accomplished by steam reforming, partial oxidation, and CO_2 reforming of methane.[12] CO_2 reforming of methane (CRM) is an attractive method to produce hydrogen-rich syngas from the reaction of carbon dioxide with hydrocarbons such as methane.[13] CRM is seen as one of the most cost-effective methods to reduce global warming and encourage chemical and energy industries to use resources more sustainably. The CRM reaction is represented by:

Chemical Engineering Department, College of Engineering, King Saud University, P. O. Box 800, Riyadh 11421, Saudi Arabia. E-mail: ankurdi12@gmail.com; Abalquraini@ksu.edu.sa; abasaeed@ksu.edu.sa; anishf@ksu.edu.sa; aidid@ksu.edu.sa; aalfatesh@ksu.edu.sa; Tel: +966-11-467-6859, +966-11-467-6856

$$CH_4 + CO_2 \rightarrow 2CO + 2H_2 \tag{1}$$
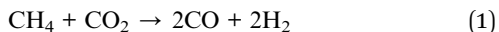
Researchers have made huge efforts to acquire appropriate catalysts for reforming catalysts to increase conversion, hydrogen yield and reduce coke formation.[14] Noble metal-based catalysts are expensive and have limited availability and researcher resorted to using transitional metals such as Ni-based catalysts.[15,16] However, Ni-based catalysts are deactivated by the sintering and deposition of carbon. Therefore, the activity and stability of performance of catalysts depend on size, support, promoters, acid–base properties, and oxidation states of the metals.[17–19] Arif et al.; used Ni/ZrO_2 and Ni/CaO catalysts for producing hydrogen via CO_2 dry reforming of glycerol.[20] Ni-based catalysts can be improved by adding basic modifiers such as MgO and CeO_2.[21] Dong et al.; reported the impact of changing the amount of nickel on the conversion of methane into syngas over $Ni/Ce–ZrO_2$ catalyst.[22] Liu et al.; employed $Ni–ZrO_2@SiO_2$ and little coking and sintering of nickel particles were noted.[23] Fakeeha et al.; studied the effect of doping La_2O_3 and WO_3 on the decomposition of methane by the Fe–Ni catalyst over the ZrO_2 support.[24] Their study revealed that the La_2O_3 doped ZrO_2 support resulted in the maximum decomposition of methane to hydrogen with relatively high stability. Zhang et al.; investigated the stabilization of the metastable structure of ZrO_2 by reflux treatment and the improvement of Ni/ZrO_2 catalyst for CRM.[25] Their results improved the stability, performance, and coke resistance of the Ni/ZrO_2 catalyst. Wang et al.; promoted the Ni/ZrO_2 catalyst with silica in CRM.[26] High conversions of CH_4 and CO_2 and long stability were accomplished. Therdthianwong et al.; examined the influence of ZrO_2 as a catalyst and promoter.[27] For CRM. They found the ZrO_2 additive fundamentally enhanced the coke resistance of Ni/Al_2O_3. Abasaeed et al.; investigated the influence of catalysts calcination temperature on the production of H_2 over ceria- and zirconia-supported cobalt catalysts in CRM.[28] Higher activity and H_2 yield resulted over the catalysts, calcined at lower temperatures, than those, calcined at higher temperatures. Wolfbeisser et al.; reported catalytic restraint of $Ce_{1−x}Zr_xO_2$, ZrO_2 and CeO_2 supported for Ni nanoparticles in CRM.[29] They found that ZrO_2 gave the best results in terms of decreasing coke formation, stability, and activity. Ibrahim et al.; examined the impact of adding phosphate (PO_4) to Ni/ZrO_2 catalyst for the CRM process.[30] They found out that the loading of Ni affected significantly the catalytic activity and stability and that phosphate was essential for promoting the catalyst. Sheng et al.; investigated the performance of Ni and Co nanoparticles within ZrO_2 hollow sphere in CRM.[31] The $Ni_{0.8}Co_{0.2}/H–ZrO_2$ catalyst displayed the highest activity and stability owing to the strong metal–support interaction phenomenon, which in turn inhibited the sintering of metal nanoparticles at high temperatures. Pompeo et al.; investigated the stability advancement on $Ni/\alpha-Al_2O_3$ catalysts improved by the addition of CeO_2 and/or ZrO_2 to produce H_2 from CRM.[32] They found that the addition of small quantities of CeO_2 and ZrO_2 to $\alpha-Al_2O_3$ upgraded the activity and stability. Al-Fakeeha et al.; tested the promoted and non-promoted 5% Co–5% $Ni/Al_2O_3–ZrO_2$ catalyst with iridium in CRM.[33] They found that the addition of Ir had a significant impact on activity by increasing the conversions of CO_2 and CH_4 by 20%, decreasing the carbon deposition, and improving the reducibility of the active catalyst. To avoid the deposition of carbon, the catalysts can be altered by the addition of promoters, being alkaline and alkaline earth metals.[34] Cao et al.; examined the effect of cerium promoter on the activity of cobalt over gamma-alumina applied in dry reforming of methane.[35] They found that the dispersion of the active metal over the support and its reducibility was markedly improved. Sha et al.; investigated the promotional effect of Ga towards the CO_2 hydrogenation to methanol.[36] Their results exhibited that the Ga promoter enhanced the adsorption and activation of H_2 and CO_2, thus improving the catalytic performance of methanol synthesis from CO_2 hydrogenation. The contributions of the previous investigators are summarized and tabulated in Table S1.†

In view of the above, it has been identified that CRM is a promising technique that produces hydrogen in an efficient way using ZrO_2 supported catalysts over a range of different materials. However, it has been a less focused area and has not been studied systematically despite its promising results in producing hydrogen. In this work, Ni-based catalysts supported on ZrO_2 will be prepared by the wet impregnation method and implemented on CRM to produce H_2 and CO. The effect of certain stabilizers such as MgO and Y_2O_3 of the support and the influence of their various loadings on the overall performance of CO_2 reforming of methane was investigated. The study also covered the use of promoters like Sr, Cs, and Ga and their impacts on the process.

2. Experimental

2.1 Materials

Nickel nitrate hexahydrate $[Ni(NO_3)_2 \cdot 6H_2O]$, gallium nitrate hydrate $[Ga(NO_3)_3 \cdot 6H_2O]$, strontium nitrate tetrahydrate $[Sr(NO_3)_2 \cdot 4H_2O]$, and cesium nitrate $[CsNO_3]$ with 99% purity was purchased from Sigma-Aldrich. The zirconia (ZrO_2) support was obtained from Anhui Elite industrial with 99% purity. Yttria $(Y_2O_3, 99.9\%)$ were bought from MKnano Co. Magnesium oxide $(MgO, 99.9\%)$ was purchased from Sigma-Aldrich. Distilled water was used for impregnation. The catalyst designation in Table S2,† preparation, testing, and characterizations are given in the support information.

3. Results

The textural properties of the fresh catalysts for both non-promoted and promoted catalysts were studied using nitrogen adsorption–desorption isotherms (Fig. 1). The results of isotherms are presented in Fig. 1A and B. In accordance with IUPAC classifications of isotherms, the isotherms are of type IV, typical of mesoporous materials, with an H3-type hysteresis loop, which resulted from capillary condensation and evaporation at high relative pressures.[37] The relative pressure increased in the range of $0.8–1.0$ P/P_0. In addition, all catalysts had low specific surface areas which were reflected by their low specific volume adsorbed of nitrogen gas, lying in the range of
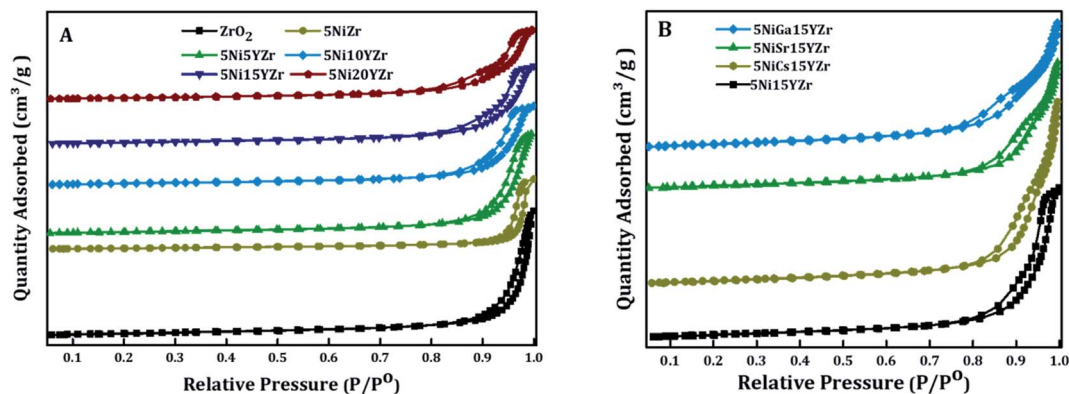
Fig. 1 N_2 adsorption–desorption isotherms curves for (A) non-promoted, (B) promoted Ni catalysts.

4.5–8.0 $cm^3 g^{-1}$. The structure of the support was not changed by the incorporation of the active metal and promoter.

Table 1 summarizes the BET surface and porosity. Sole ZrO_2 support showed a specific surface area of 21 $m^2 g^{-1}$, which decreased to 16 $m^2 g^{-1}$ upon impregnation of NiO, an indication of the successful loading process onto the surface of the support. However, the pore size increased from 37 nm for meso-ZrO_2 to 42 nm after loading NiO because of the decomposition of nickel(II) nitrate hexahydrate and evolution of H_2O, NO_2, HNO_3, and O_2 gases during the calcination step.[38] The BET surface area of the catalysts increased when the Y_2O_3 was added and this was associated with the decrease of the NiO crystal size, shown by the XRD results in Table 1, and the creation of O_2 vacancy.[39] The incorporation of promoters enhanced the BET by providing extra active sites, while the pore volume and size remained almost the same (Table 1).

Fig. 2 displays the reducibility of the catalysts using H_2-TPR analysis. In general, all samples have the same classification which is bimodal at 250–550 °C, but with different patterns, and the amounts of hydrogen consumed for the reduction are shown in Fig. 3. After 600 °C there is no more NiO left to reduce. 5NiZr catalysts have a unique reduction behavior and the highest reduction peak at 434 °C with high hydrogen consumption. Primarily, the nature of support material dominates the extent of synergy that exists within catalyst components. Adding the Y_2O_3 to the support significantly affected the reduction in terms of temperature range and hydrogen consumption. When the Y_2O_3 load is less or equal to 10 wt%,

the interaction between the active metal and support increases, thus shifting the peaks to higher temperatures. On the contrary, if the Y_2O_3 load is more than 10 wt%, suitable interaction between the Ni and support at medium temperature ranges was obtained. The Y_2O_3 load catalysts have higher hydrogen consumptions than that of 5NiZr catalysts at the lower zone indicating the presence of freer NiO species.
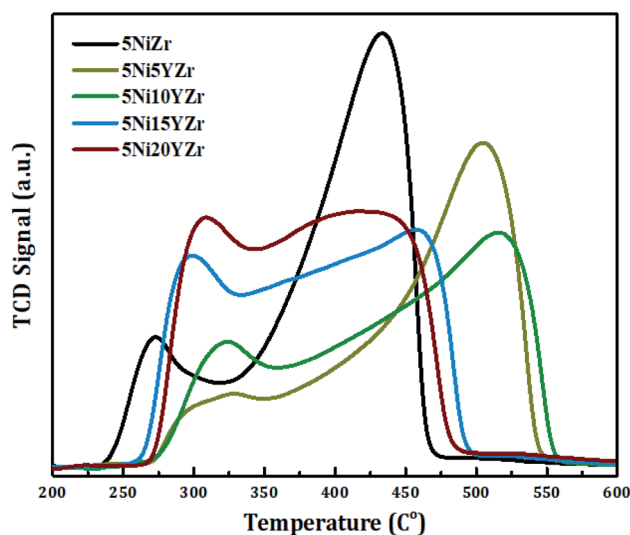

Fig. 2 H_2-TPR profiles of the synthesized catalysts.

Table 1 The textural aspect of the catalysts

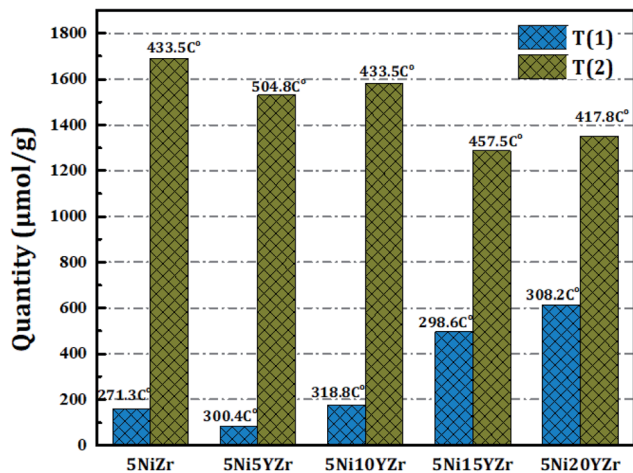| Catalyst	BET surface area ($m^2 g^{-1}$)	Pore volume (PV) ($cm^3 g^{-1}$)	Pore size (nm)	NiO crystal size (nm)
ZrO_2	21	0.16	37	—
5NiZr	16	0.15	42	31.6
5Ni5YZr	27	0.23	31	15.8
5Ni10YZr	23	0.19	25	15.8
5Ni15YZr	25	0.18	24	13.8
5Ni20YZr	24	0.17	22	16.4
5NiCs15YZr	28	0.20	28.4	—
5NiGa15YZr	30	0.15	20.0	—
5NiSr15YZr	26	0.14	23	—

Fig. 3 The quantity of hydrogen consumption during TPR analysis.

The catalytic basicity has a strong effect on CRM reaction and therefore the acidity of the prepared catalysts is determined using the CO_2-TPD technique as shown in Fig. 4. The area of CO_2 desorption peak and temperature range determines the basicity strength which is weak (50–200 °C), medium (200–400 °C), strong (400–650 °C), very strong (>650 °C).[40,41] The CO_2-TPD profiles show the CO_2 desorption peaks fall in the weak and medium zones. With the exception of 5Ni10YZr and 5Ni15YZr catalysts, where the CO_2 desorption peaks appeared in the very strong range at 665 °C. These desorption peaks are accredited to strength basic sites.[42] Based on these results, the basicity order is as follows: 5Ni15YZr > 5Ni10YZr > 5Ni5YZr > 5NiZr > 5Ni20YZr. The catalytic activity was enhanced by homogenous scatter of surface acid-basic sites, consequently lowering the tendency of coke deposition.

Fig. 5 shows the XRPD patterns of synthesized catalysts at $2\theta°$ = 5–80°. The XRPD pattern demonstrates only one crystalline phase formation of ZrO_2. The patterns are identical, but the

intensity decreases with the increase in Y_2O_3 due to the reduction in the size of the NiO crystal, and the Y_2O_3 peaks appear clearly as the loading increases. The size of NiO crystals tabulated in Table 1 is determined by the Debye–Scherrer equation. Upon analyzing diffraction data using MDI Jade® software (version 6.5, Materials Data Inc., Newtown Square, PA, USA). The monoclinic phase of ZrO_2 is identified at 24.17, 28.14, 31.47, 34.25, 38.58, 40.89, 44.87, 49.24, 54, 55.40, 57.25, 58, 60, 62.70, 65, 69, 71.30, 75 and 79° (JCPDS 81-1314)[43] while NiO diffraction peaks are identified at 35.34 and 45.5° (JCPDS 65-5745).[44] The quantity of NiO is so small in the presence of ZrO_2 support and hence its peaks are totally overlapped by those of ZrO_2. The Y_2O_3 peaks are identified at 29.20, 31, and 50.20° (JCPDS 89-5592).[45] The Y_2O_3 peaks exhibit similar features to that of NiO. However, when its loading goes beyond 10% small distinct peaks begin to appear. Scherrer's equation was employed to compute the crystallite size, which can be described as follows:

$$D_{\mathrm{p}} = K \times \lambda/\beta \cos\theta \qquad (2)$$

in which, D_{p} is the crystallite size in nanometers, K is the shape factor which is 0.94, λ is the wavelength of X-ray, β is the full width at half maximum of the diffraction peak of the sample, and θ is the diffraction angle in degrees.

The modification of the support structure by adding appropriate modifiers influences the catalytic performance. In this work, two modifiers (MgO and Y_2O_3) were used as stabilizers for the zirconia support due to their potential advantages. Five weight% of the modifiers were considered separately. Fig. 6 exhibits the catalytic performance in terms of H_2-yield versus time on stream. The result displays that the initial H_2-yield of 5NiZr, 5Ni5MgZr, and 5NiYZr are 41, 24, and 51% respectively. While the average conversion for 440 min time stream of 5NiZr, 5Ni5MgZr, and 5NiYZr are 36, 23, and 47% respectively. From
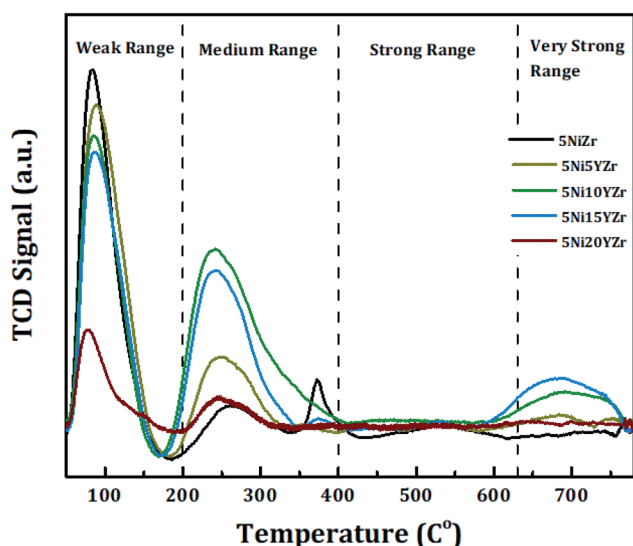

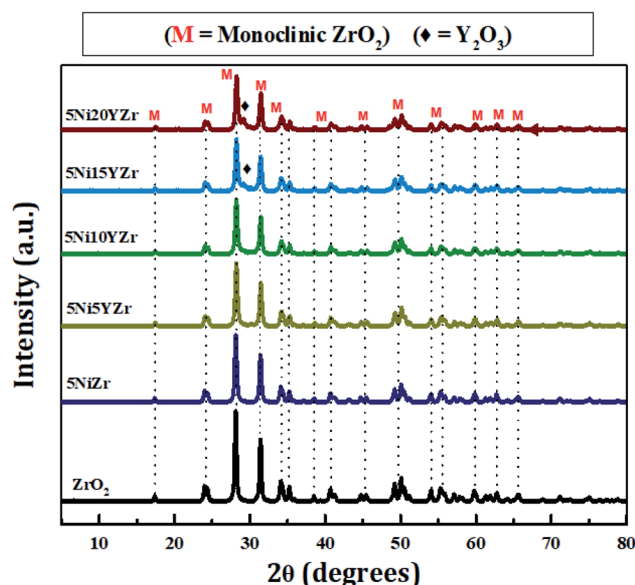Fig. 4 CO_2-TPD patterns of prepared catalysts.

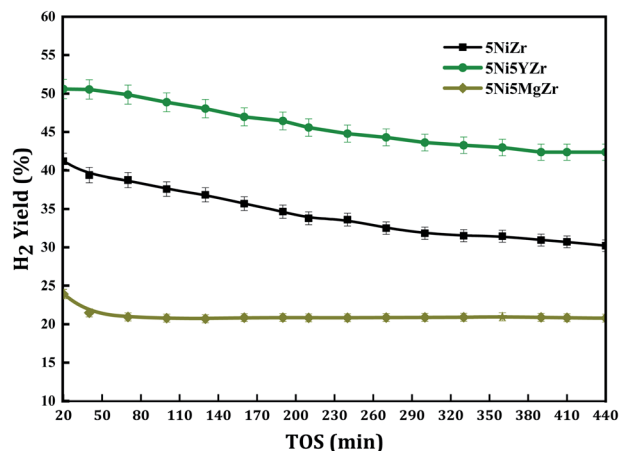

Fig. 5 The XRPD patterns of synthesized catalysts.

Fig. 6 H_2-yield% *versus* time on stream for stabilized-zirconia catalysts at a reaction temperature of 700 °C.

the figure, it is obvious that the incorporation of modifiers alters the activity performance. The Mg modifier inhibits the reaction and decreased the H_2-yield by about 36%, while the Y modifier increased about 31% over the pristine support (Zr). Having seen that the Y modifier is better than Mg one, it is plausible to check the different loadings of Y to find out the optimum.

Normally, CH_4 adsorption on reduced Ni surface is the rate-determining step for CRM, which is promoted by stable H_2 atoms adsorption on strong H_2 binding sites of the reduced Ni atom. Fig. 7 shows the H_2 yield over 440 min of reaction. The conversion of the 5Ni15YZr catalyst has the highest hydrogen yield compared to the other catalysts. The hydrogen yield profile is in this decreasing order 5Ni15YZr > 5Ni10YZr > 5Ni5YZr > 5Ni20YZr > 5NiZr. The figure displays that the H_2 yield increases with the Y_2O_3 load up to 15 wt% due to the interaction of the active metal and its dispersion in the pores of the support. On the other hand, increasing the Y_2O_3 load to 20 wt% leads to a significant decrease in the activity of the
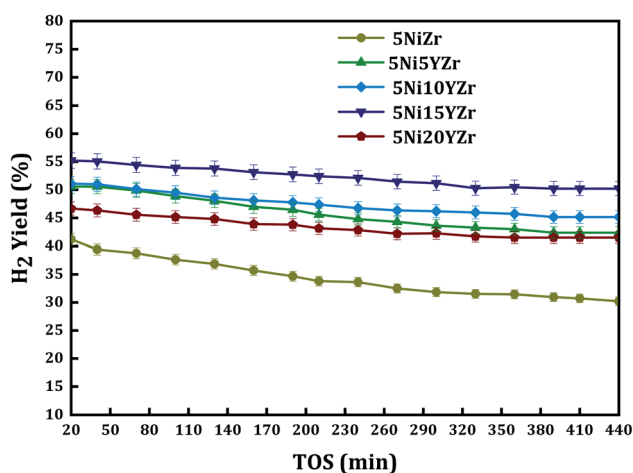
catalyst even lower than that of 5 wt%. Several researchers[46–49] have studied similar systems where the impact of lanthanide metal oxides and alkaline earth to the active metals supported on them brings the appearance of surface oxygen vacancies. The coke formation is the main reason for the inactivity of the catalyst due to blockage of the pores of the catalyst and stopping the feed flow through it.

For the quantification of carbon deposited, TGA analysis of the used catalysts obtained after 440 min of reaction was carried out as shown in Fig. 8. The weight loss started at 470 °C due to the combustion of carbon formed on the surface of the catalyst, which had a huge role in inhibiting the activity of the catalysts.[50] The percentage of weight loss equals the percentage of the amount of carbon formed. However, the addition of Y_2O_3 to 5NiZr at low loading (0.0, 5.0, 10.0, and 15.0 wt%) did not significantly influence the carbon deposition and thus, the enhancement due to the Y_2O_3 may be attributed to the reduction of active metal agglomeration. On the other hand, the high loading sample 5Ni20YZr gave quite less carbon formation. The order of the weight loss% of the samples is as follows: 5Ni5YZr > 5Ni10YZr > 5Ni15YZr > 5NiZr > 5Ni20YZr.

For a better understanding of morphology and carbon formation, TEM was performed in Fig. 9. The TEM micrographs of the best (5Ni15YZr) and the basic (5NiZr) catalysts were analyzed using both fresh and used samples. It is shown for fresh samples that the promoted catalyst has better distribution and smaller active metal particles size, while for spent samples, 5NiZr exhibits sintering and bulky layers due to the increase in the particle size of the nickel. Whereas the 5Ni15YZr contains slim layers of multiwall carbon nanotubes.

The performance Ni supported on stabilized zirconia is further upgraded by incorporation of active metal with elements like (Cs, Ga, and Sc). Fig. 10 illustrates the catalytic performance of H_2-yield% against the time on stream performance. In this work, a fixed 3 wt% of promoters were adopted. The result displays that the initial H_2-yield of 5Ni15YZr, 5Ni15CsYZr, 5Ni15GaYZr, and 5Ni15SrYZr are 55.3, 56.6, 60.6, and 63.4%

Fig. 7 H_2 yield% *versus* time on stream for different loading of yttria-stabilized-zirconia catalysts at a reaction temperature of 700 °C.
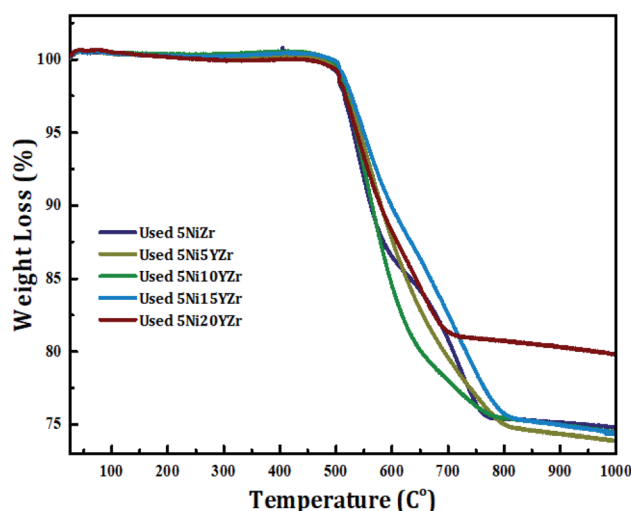

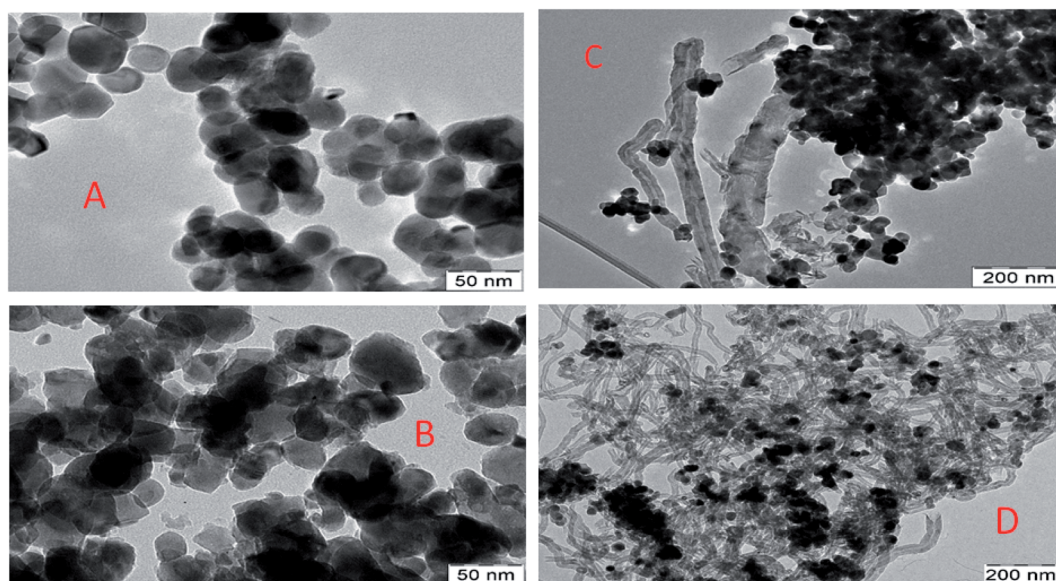Fig. 8 TGA profile for spent catalysts at 700 °C.

Fig. 9 TEM micrographs and matching particle size distribution: (A) and (B) for fresh and (C) and (D) for spent catalysts of 5NiZr, and 5Ni15YZr respectively at a reaction temperature of 700 °C.
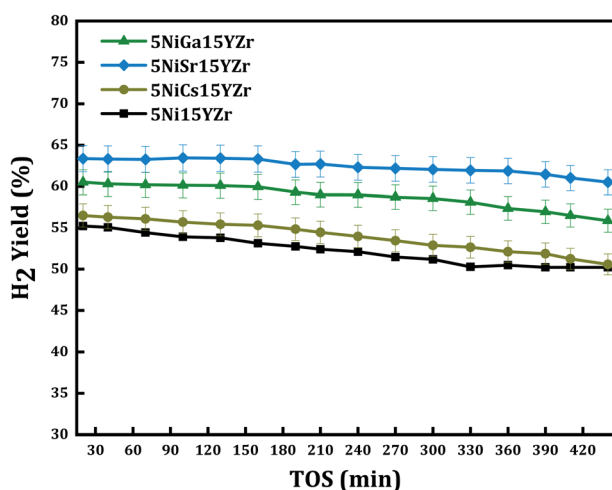

Fig. 10 H$_2$ yield% *versus* time on stream for different promoters of yttria-stabilized-zirconia catalysts at a reaction temperature of 700 °C.

respectively. The Cs, Ga, and Sr promoters enhanced the H$_2$-yield% by 3%, 12.5%, and 19% respectively over the non-promoted "5Ni15YZr". Thus, the 5Ni15SrYZr catalyst outperforms all other catalysts and hence generates the highest average H$_2$-yield% of 62%. The work of previous investigators is compared with the present one as shown in Table 2. It is evident that the present catalyst provides a higher hydrogen yield than those catalysts operated at the same reaction temperature of 700 °C.

The TGA analysis was performed for the used promoted catalysts obtained after 440 min of reaction. Fig. 11 displays the % weight loss profiles. The produced carbon is in line with the activity of the promoted catalysts. Therefore, the most reactive promoted catalyst (5Ni15SrYZr) generates the highest amount of carbon (9.7% weight loss) while the least reactive catalyst (5Ni15CsYZr) promoted catalyst produced the minimum carbon deposition (2.6% weight loss). All promoted catalysts revealed less carbon deposition compared to the non-promoted catalyst (5Ni15YZr) which gives 25.6% weight loss.

Table 2 Performance comparison results

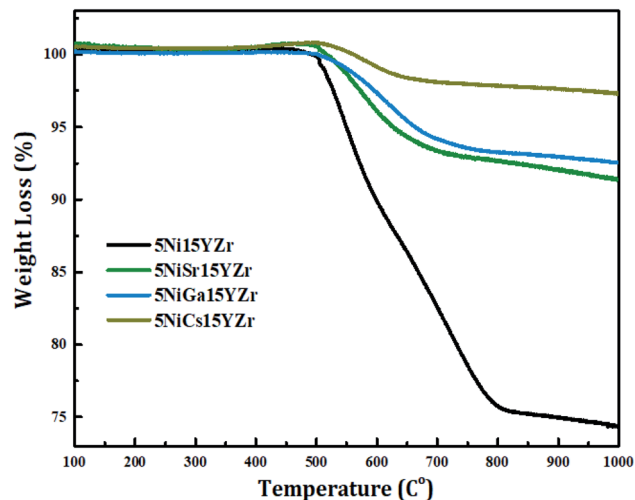| Catalyst	Wt. (g)	Tr	GHSV (L g^{-1} h^{-1})	Y (%)	Ref.
NiSr/Y$_2$O$_3$–ZrO$_2$	0.1	700	42	62	This work
Ni5Ce/La$_2$O$_3$–ZrO$_2$	0.1	800	42	85	51
Ni2Ce/Y$_2$O$_3$ZrO$_2$	0.1	800	28	80	52
Ni–Si/ZrO$_2$	0.25	450	14.4	4.3	26
Ni–Zr/SiO$_2$	0.25	450	14.4	3.5	26
Ni@ZrO$_2$–SiZr-7.7	0.1	800	72	81	53
0.8% Ni + 0.2% Co–MgAl$_2$O$_4$	0.5	700	54	51	54
10Ni + 1% Fe–MgAl$_2$O$_4$	0.1	750	30	78	55
Ni–Pd/SiO$_2$-Imp.	0.1	700	24	45	56
Ni/CeO$_2$–ZrO$_2$	0.1	700	30	33	57
Ni/L$_2$O$_3$ + CeO$_2$	0.15	800	40	40	58

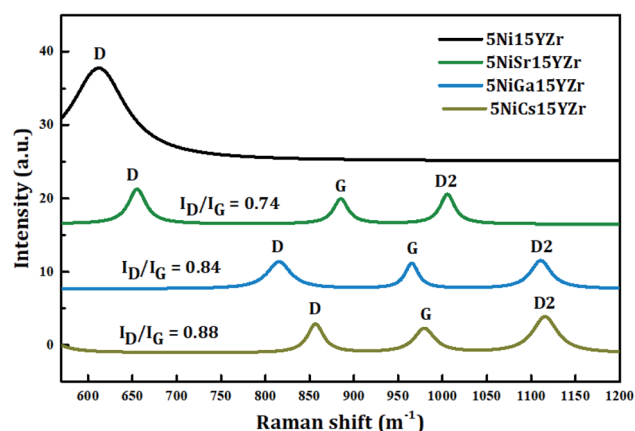Fig. 11 TGA profile for promoted spent catalysts at 700 °C.

Fig. 12 Raman spectra for the used promoted catalysts.

Raman spectroscopic analysis was carried out to reveal the structure of carbon deposits over the spent catalysts. Fig. 12 displays the Raman spectra of the used promoted catalysts. The Raman study indicates a structural change in 5Ni15YZr after the incorporation of promoters. 5NiGa15YZr and 5NiCs15YZr catalysts depict three bands with Raman shifts in the range of 816–857 cm^{-1}, 966–979 cm^{-1} and 1112–1115 cm^{-1}, while the three bands of NiSr15YZr catalyst, somewhat shifted to the lower values of Raman shift, appear at 654 cm^{-1}, 885 cm^{-1}, and 1006 cm^{-1}. The non-promoted catalyst (5Ni15YZr) displays a single peak in a similar range at 612 cm^{-1}. The three weak peaks for the promoted catalyst can be ascribed to the induced disorders in the graphite (D), the ideal vibration of the graphite layers (G), and the overtone of the D band (D2).[59] Normally, the intensity ratio of the D band to the G band (*i.e.* I_D/I_G) provides the extent of the crystalline order of graphite in carbonaceous materials.[60] Values of ratios obtained are 0.84, 0.88, and 0.74 for 5NiGa15YZr, 5NiCs15YZr, and 5NiSr15YZr catalysts respectively, indicating a high degree of graphitization.

4. Conclusions

Hydrogen production *via* DRM was investigated over a 5Ni/ZrO$_2$ catalyst. The effect of Y$_2$O$_3$ modifier loading (*i.e.*, 0.0, 5.0, 10.0, 15.0, 20.0 wt%), were examined. All catalysts gave low specific surface areas in accordance with their low specific volume adsorption of N$_2$. But, the BET surface area of the catalysts increased when the modifiers and promoters were added. Both in the H$_2$-TPR and CO$_2$-TPD analysis, the addition of Y$_2$O$_3$ had a positive effect as it lowered the temperature of reduction and reduced hydrogen consumption during the activation process, and increased the basicity. On the other hand, increasing the Y$_2$O$_3$ modifier improved the catalytic performance, hydrogen production, and reduced carbon deposition. The 15 wt% Y$_2$O$_3$ catalyst (5Ni15YZr) was found to be the optimum. The TEM analysis displayed the formation of nano-filament containing multiwall carbon nanotubes. The promotion of the catalysts brought about reduction in carbon deposition. The promoting effects of Ni supported on 15 wt% Y$_2$O$_3$ displayed that Sr promoter was better than Cs and Ga promoters. The Raman analysis of used promoted catalysts depicted the different forms of carbon deposited and the dominance of the graphitic structure.

5. Recommendations

The hydrogen production, over the 5Ni/ZrO$_2$ catalyst *via* DRM investigated, was prepared using the impregnation technique. Therefore, it suggested the catalysts be prepared by other methods so as to compare them. The variation of operating conditions is also recommended, by testing higher reaction temperatures of the obtained best catalyst. The utilization of different stabilizers and promoters is recommended. Moreover, the study of the kinetics and the mechanism of the system used is recommended. Finally, the use of other cost-effective active elements such as Co or their combination with Ni is recommended.

Conflicts of interest

There are no conflicts to declare.

Acknowledgements

References

1 F. Martins, C. Felgueiras, M. Smitkova and N. Caetano, *Energies*, 2019, **12**, 964.
2 S. Oros-Ruiz, R. Zanella, R. López, A. Hernández-Gordillo and R. Gómez, *J. Hazard. Mater.*, 2013, **263**, 2–10.
3 A. Tiwari, *Adv. Mater. Lett.*, 2021, **12**(10), 1–5.
4 T. Stangarone, *Clean Technol. Environ. Policy*, 2020, **23**, 509–516.
5 A. Azadeh and S. Tarverdian, *Energy Policy*, 2007, **35**(10), 5229–5241.

6 G. Aydin, S. Kaya and I. Karakurt, *Proceedings of the 24th International Mining Congress and Exhibition Of Turkey, IMCET 2015*, Antalya, Turkey, April 14-17, 2015.

7 G. Aydin, I. Karakurt and K. Aydiner, *Energy Sources, Part A*, 2012, **34**, 967–982.

8 M. Momirlan and T. Veziroğlu, *Renewable Sustainable Energy Rev.*, 1999, **3**, 219–231.

9 S.-H. Liu and H.-R. Syu, *Appl. Energy*, 2012, **100**, 148–154.

10 M. G. A. Rubio and K. Jaojaruek, *2016 International Conference on Cogeneration, Small Power Plants and District Energy*, 2016, DOI: 10.1109/COGEN.2016.7728949.

11 M. Hirscher, T. Autrey and S.-i. Orimo, *ChemPhysChem*, 2019, **20**, 1157.

12 R. J. Press, K. S. V. Santhanam, M. J. Miri, A. V. Bailey and G. A. Takacs, *ChemSusChem*, 2009, **2**, 781.

13 A. Al-Fatesh, S. K. Singh, G. S. Kanade, H. Atia, A. H. Fakeeha, A. A. Ibrahim, A. M. El-Toni and N. K. Labhasetwar, *Int. J. Hydrogen Energy*, 2018, **43**, 12069–12080.

14 W.-J. Jang, J.-O. Shim, H.-M. Kim, S.-Y. Yoo and H.-S. Roh, *Catal. Today*, 2019, **324**, 15–26.

15 A. Steinfeld, *Int. J. Hydrogen Energy*, 2002, **27**, 611–619.

16 J. Xu, W. Zhou, Z. Li, J. Wang and J. Ma, *Int. J. Hydrogen Energy*, 2009, **34**, 6646–6654.

17 L. Chen, Z. Qi, S. Zhang, J. Su and G. A. Somorjai, *Catal*, 2020, **10**, 858.

18 Z. Zuo, S. Liu, Z. Wang, C. Liu, W. Huang, J. Huang and P. Liu, *ACS Catal.*, 2018, **8**, 9821–9835.

19 D. P. Harrison, in *Industrial and Engineering Chemistry Research*, American Chemical Society, 2008, vol. 47, pp. 6486–6501.

20 N. N. M. Arif, D.-V. N. Vo, M. T. Azizan and S. Z. Abidin, *Bull. Chem. React. Eng. Catal.*, 2016, **11**, 200–209.

21 M.-S. Fan, A. Z. Abdullah and S. Bhatia, *Int. J. Hydrogen Energy*, 2011, **36**, 4875–4886.

22 W.-S. Dong, H.-S. Roh, K.-W. Jun, S.-E. Park and Y.-S. Oh, *Appl. Catal., A*, 2002, **226**, 63–72.

23 W. Liu, L. Li, X. Zhang, Z. Wang, X. Wang and H. Peng, *J. CO2 Util.*, 2018, **27**, 297–307.

24 A. H. Fakeeha, S. O. Kasim, A. A. Ibrahim, A. S. Al-Awadi, E. Alzahrani, A. E. Abasaeed, A. E. Awadallah and A. S. Al-Fatesh, *Front. Chem.*, 2020, **8**, 317.

25 M. Zhang, J. Zhang, X. Zhang, Z. Zhou, F. Song, Q. Zhang, Y. Tan and Y. Han, *Energy Convers. Manage.*, 2020, **216**, 112950.

26 Y. Wang, L. Yao, Y. Wang, S. Wang, Q. Zhao, D. Mao and C. Hu, *ACS Catal.*, 2018, **8**, 6495–6506.

27 S. Therdthianwong, A. Therdthianwong, C. Siangchin and S. Yongprapat, *Int. J. Hydrogen Energy*, 2008, **33**, 991–999.

28 A. E. Abasaeed, A. S. Al-Fatesh, M. A. Naeem, A. A. Ibrahim and A. H. Fakeeha, *Int. J. Hydrogen Energy*, 2015, **40**, 6818–6826.

29 A. Wolfbeisser, O. Sophiphun, J. Bernardi, J. Wittayakun, K. Fottinger and G. Rupprechter, *Catal. Today*, 2016, **277**, 234–245.

30 A. A. Ibrahim, A. S. Al-Fatesh, W. U. Khan, S. O. Kasim, A. E. Abasaeed, A. H. Fakeeha, G. Bonura and F. Frusteri, *Int. J. Hydrogen Energy*, 2019, **44**, 27784–27794.

31 K. Sheng, D. Luan, H. Jiang, F. Zeng, B. Wei, F. Pang and J. Ge, *ACS Appl. Mater. Interfaces*, 2019, **11**, 24078–24087.

32 F. Pompeo, D. Gazzoli and N. N. Nichio, *Int. J. Hydrogen Energy*, 2009, **34**, 2260–2268.

33 A. H. Fakeeha, A. A. Ibrahim, Y. Arafat, H. Atia, A. E. Abasaeed and A. S. Al-Fatesh, *Can. J. Chem. Eng.*, 2018, **96**, 955–960.

34 R. Franz, R. Franz, T. Kühlewind, G. Shterk, E. Abou-Hamad, A. Parastaev, E. Uslamin, E. J. M. Hensen, F. Kapteijn, J. Gascon and E. A. Pidko, *Catal. Sci. Technol.*, 2020, **10**, 3965–3974.

35 A. N. T. Cao, C. Q. Pham, L. K. H. Pham, D. Le Tri Nguyen, P. T. T. Phuong, T. T. V. Tran, V.-P. Nguyen, T. B. Nguyen, Q. Van Le, N. A. Nguyen and T. M. Nguyen, *Int. J. Hydrogen Energy*, DOI: 10.1016/j.ijhydene.2021.11.077.

36 F. Sha, C. Tang, S. Tang, Q. Wang, Z. Han, J. Wang and C. Li, *J. Catal.*, 2021, **404**, 383–392.

37 D. M. Oliveira and A. S. Andrada, *Cerâmica*, 2019, **65**, 170–179.

38 W. Brockner, C. Ehrhardt and M. Gjikaj, *Thermochim. Acta*, 2007, **456**, 64–68.

39 P. J. B. Marcos and D. Gouvêa, *Cerâmica*, 2004, **50**, 38–42.

40 A. S. Al-Fatesh, M. A. Naeem, A. H. Fakeeha and A. E. Abasaeed, *Bull. Chem. Soc. Jpn.*, 2013, **86**, 742–748.

41 M. A. Naeem, A. S. Al-Fatesh, A. E. Abasaeed and A. H. Fakeeha, *Fuel Process. Technol.*, 2014, **122**, 141–152.

42 A. H. Fakeeha, A. S. Al Fatesh, A. A. Ibrahim, A. N. Kurdi and A. E. Abasaeed, *ACS Omega*, 2021, **6**, 1280–1288.

43 P. R. Rauta, P. Manivasakan, V. Rajendran, B. B. Sahu, B. K. Panda and P. Mohapatra, *Phase Transitions*, 2012, **85**, 13–26.

44 H. Lu, M. Zheng, J. Chen, N. Li, L. Xue and J. Cao, *Integr. Ferroelectr.*, 2011, **127**, 128–133.

45 H.-Y. Jung, H.-J. Kim, S. Yang, Y.-G. Kang, B.-Y. Oh, H.-G. Park and D.-S. Seo, *Liq. Cryst.*, 2012, **39**, 789–793.

46 W.-P. Dow, Y.-P. Wang and T.-J. Huang, *Appl. Catal., A*, 2000, **190**, 25–34.

47 W.-P. Dow and T.-J. Huang, *J. Catal.*, 1996, **160**, 171–182.

48 K. Kawamura, K. Watanabe, T. Hiramatsu, A. Kaimai, Y. Nigara, T. Kawada and J. Mizusaki, *Solid State Ionics*, 2001, **144**, 11–18.

49 J. B. Wang, Y.-L. Tai, W.-P. Dow and T.-J. Huang, *Appl. Catal., A*, 2001, **218**, 69–79.

50 X. Du, L. J. France, V. L. Kuznetsov, T. Xiao, P. P. Edwards, H. AlMegren and A. Bagabas, *Appl. Petrochem. Res.*, 2014, **4**, 137–144.

51 J. Khatri, A. S. Al-Fatesh, A. H. Fakeeha, A. A. Ibrahim, A. E. Abasaeed, S. O. Kasim, A. I. Osman, R. Patel and R. Kumar, *Mol. Catal.*, 2021, **504**, 111498.

52 A. H. Fakeeha, A. S. Al Fatesh, A. A. Ibrahim, A. N. Kurdi and A. E. Abasaeed, *ACS Omega*, 2021, **6**, 1280–1288.

53 Z. Y. Lim, J. Tu, Y. Xu and B. Chen, *J. Colloid Interface Sci.*, 2021, **590**, 641–651.

54 M. H. Aghaali and S. Firoozi, *Int. J. Hydrogen Energy*, 2021, **46**, 357–373.

55 R. L. B. A. Medeiros, H. P. Macedo, V. R. M. Melo, Â. A. S. Oliveira, J. M. F. Barros, M. A. F. Melo and D. M. A. Melo, *Int. J. Hydrogen Energy*, 2016, **41**, 14047–14057.

56 C. Pan, Z. Guo, H. Dai, R. Ren and W. Chu, *Int. J. Hydrogen Energy*, 2020, **45**, 16133–16143, DOI: 10.1016/j.ijhydene.2020.04.066.

57 A. Kambolis, H. Matralis, A. Trovarelli and C. Papadopoulou, *Appl. Catal., A*, 2010, **377**, 16–26.

58 N. D. Charisiou, G. Siakavelas, L. Tzounis, V. Sebastian, A. Monzon, M. A. Baker, S. J. Hinder, K. Polychronopoulou, I. V. Yentekakis and M. A. Goula, *Int. J. Hydrogen Energy*, 2018, **43**, 18955–18976.

59 S. Reich and C. Thomsen, *Philos. Trans. R. Soc., A*, 2004, **362**, 2271–2288.

60 Y. Kameya and K. Hanamura, *Chem. Eng. J.*, 2011, **173**, 627–635.